AVE 0991 attenuates oxidative stress and neuronal apoptosis via Mas/PKA/CREB/UCP-2 pathway after subarachnoid hemorrhage in rats

Jun Mo[a,b,c], Budbazar Enkhjargal[b], Zachary D. Travis[d], Keren Zhou[b,c], Pei Wu[b], Guangyu Zhang[e], Qiquan Zhu[b], Tongyu Zhang[b], Jianhua Peng[b], Weilin Xu[b,c], Umut Ocak[b], Yili Chen[a], Jiping Tang[b], Jianmin Zhang[a,c,f,*], John H. Zhang[b,g,h,**]

[a] Department of Neurosurgery, The Fourth Affiliated Hospital, Zhejiang University School of Medicine, Yiwu 322000, Zhejiang, China
[b] Department of Physiology and Pharmacology, Loma Linda University, Loma Linda, CA 92350, USA
[c] Department of Neurosurgery, The Second Affiliated Hospital, Zhejiang University School of Medicine, Hangzhou 310009, Zhejiang, China
[d] Department of Earth and Biological Sciences, Loma Linda University, Loma Linda, CA 92350, USA
[e] Mass Spectrometry Core Facility, Loma Linda University, Loma Linda, CA 92350, USA
[f] Brain Research Institute, Zhejiang University, Hangzhou 310000, Zhejiang, China
[g] Department of Anesthesiology, Loma Linda University, Loma Linda, CA 92350, USA
[h] Department of Neurosurgery, Loma Linda University, Loma Linda, CA 92350, USA

ARTICLE INFO

ABSTRACT

Oxidative stress and neuronal apoptosis have been demonstrated to be key features in early brain injury (EBI) after subarachnoid hemorrhage (SAH). Previous studies have indicated that Mas receptor activation initiates an anti-oxidative and anti-apoptotic role in the brain. However, whether Mas activation can attenuate oxidative stress and neuronal apoptosis after SAH remains unknown. To investigate the beneficial effect of Mas on oxidative stress injury and neuronal apoptosis induced by SAH, a total of 196 rats were subjected to an endovascular perforation model of SAH. AVE 0991 (AVE), a selective agonist of Mas, was administered intranasally 1 h after SAH induction. A779, a selective inhibitor of Mas, and small interfering ribonucleic acid (siRNA) for UCP-2 were administered by intracerebroventricular (i.c.v) injection at 1 h and 48 h before SAH induction respectively. Neurological tests, immunofluorescence, TUNEL, Fluoro-Jade C, DHE staining, and Western blot experiments were performed. We found that Mas activation with AVE significantly improved neurobehavioral scores and reduced oxidative stress and neuronal apoptosis in SAH + AVE group compared with SAH + vehicle group. Moreover, AVE treatment significantly promoted phosphorylation of CREB and the expression UCP-2, as well as upregulated expression of Bcl-2 and downregulation of Romo-1 and Bax. The protective effects of AVE were reversed by i.c.v injection of A779 and UCP-2 siRNA in SAH + AVE + A779 and SAH + AVE + UCP-2 siRNA groups, respectively. In conclusion, our data provides evidence that Mas activation with AVE reduces oxidative stress injury and neuronal apoptosis through Mas/PKA/p-CREB/UCP-2 pathway after SAH. Furthermore, our study indicates that Mas may be a novel therapeutic treatment target in early brain injury of SAH.

1. Introduction

Early brain injury (EBI) occurring within 72 h has been proposed to be a major cause of the poor outcomes seen in patients who suffer a subarachnoid hemorrhage (SAH) event [1–3]. Oxidative stress and neuronal apoptosis have been revealed to contribute to the irreversible acute brain injury after SAH insult [4,5]. An imbalance that favors the production of reactive oxygen species (ROS) versus the neutralization by intrinsic antioxidant systems has been demonstrated in the brain following SAH in both experimental animal models and human [5–7]. Furthermore, excessive free radicals can lead to neuronal damage by either the initiation of apoptotic cascades or by leading the cells into necrosis through mitochondrial-mediated mechanism [8–10].

Mitochondria have been considered as the main source of ROS due

---

to an ischemic disruption of the electron transfer chain following SAH [5]. ROS has also been shown to induce apoptosis by increasing p53, inducing cytochrome c release and activating caspase-9 and caspase-3 [8,11]. Recently, increasing evidence has indicated that uncoupling protein-2 (UCP-2) can lead to a mild uncoupling by decreasing electrical potential between intermembrane space and matrix of mitochondria, which can dramatically reduce the production of ROS [12,13]. The hypothesis of 'uncoupling to survive' associated with UCP-2 has been further demonstrated in the models of traumatic brain injury and ischemic stroke [12,14,15]. However, the precise mechanism of UCP-2 regulation on ROS production still remains unclear.

Mas is a G-protein coupled receptor which is highly expressed in the brain and has been identified as a new component of the brain renin-angiotensin system (RAS) [16]. The neuroprotective effect of Mas in the central nervous system (CNS) injuries has been elucidated in the recent study, which was associated with antioxidant and anti-apoptotic properties [17]. Continuous intracerebroventricular (i.c.v) administration of Angiotensin-(1−7)[Ang-(1−7)], an endogenous ligand of Mas, can decrease infarct size and neurological deficit at 72 h after occlusion in endothelin-1-induced middle cerebral artery occlusion (MCAO) model [18,19]. Although the precise mechanism by which Ang-(1−7) exerts its neuroprotective actions is not clear, it seems to involve the activation of Mas and modulation on oxidative stress, apoptosis, and inflammation [20]. Moreover, Ang-(1−7) has a very short half-life, as a result of its peptidic nature, which limits its clinical applications [21].

Fortunately, a non-peptide analogue of Ang-(1−7) called AVE 0991 (AVE) with a prolonged half-life time and highly specific binding to Mas was found recently [22,23]. AVE, 5-Formyl-4-methoxy-2-phenyl-1-[[4-[2-(ethylaminocarbonylsulfonamido)−5-isobutyl-3-thienyl]-phenyl]-meth-yl]-imidazole, is a substituted imidazole derivative that has previously been shown to be a selective agonist of Mas [23]. This compound mimics the effects of Ang-(1−7) in the blood vessels [23,24], brain [25], and kidney [26] and also has shown to have possess protective properties including antioxidant, anti-apoptotic and anti-inflammatory. However, the effects of AVE on oxidative stress and neuronal apoptosis in EBI after SAH have not been investigated. In the current study, we assessed the hypothesis that AVE attenuates oxidative stress and neuronal apoptosis through Mas/PKA/CREB/UCP-2 pathway in EBI after SAH in rats.

2. Materials and methods

2.1. Animals

All experimental procedures were approved by the Institutional Animal Care and Use Committee (IACUC) of Loma Linda University and were in accordance with the NIH Guidelines for the Use of Animals in Neuroscience Research. All experiments were reported with the ARRIVE (Animal Research: Reporting In Vivo Experiments) guidelines for reporting in vivo experiments. One hundred and ninety-six male Sprague-Dawley rats weighing 280–320 g were used. All rats were housed in a controlled humidity and temperature room with a 12 h light and dark cycle and raised with free access to water and food.

2.2. Study design

Four separated experiments were conducted as follows (Fig. s1).

2.2.1. Experiment 1

To study the temporal expression and cellular localization of Mas receptor, 36 rats were randomly divided and assigned to six groups: Sham (n = 6), SAH-3 h (n = 6), SAH-6 h (n = 6), SAH-12 h (n = 6), SAH-24 h (n = 6), SAH-72 h (n = 6). Western blot analysis was performed to determine the expression changes of Mas. An additional 4 rats in the Sham (n = 2) and SAH-24 h (n = 2) groups were used for double immunofluorescence staining.

2.2.2. Experiment 2

To evaluate the effects of AVE on short-term outcome after SAH, 40 rats were randomly divided and assigned to five groups: Sham (n = 8), SAH + vehicle (10% DMSO dissolved in corn oil, n = 10), SAH + AVE (0.3 mg/kg, n = 6), SAH + AVE (0.9 mg/kg, n = 10), and SAH + AVE (2.7 mg/kg, n = 6). SAH grade and neurological performance were assessed at 24 h after SAH. Based on the results of neurological tests, AVE (0.9 mg/kg)-treated group of SAH rats were used for Western blot, Fluoro-Jade C, TUNEL, and DHE staining to evaluate oxidative stress and neuronal apoptosis in the ipsilateral hemisphere at 24 h after SAH. An additional 4 rats were randomly divided and assigned into naive + AVE (0.9 mg/kg, n = 2) and naive + vehicle (10% DMSO dissolved in corn oil, n = 2) groups. Determination of AVE in the brain using mass spectrum analysis was performed at 6 h after drug administration by intranasal route.

2.2.3. Experiment 3

To evaluate the effects of AVE on long-term outcome after SAH, 29 rats were randomly divided and assigned into three groups: Sham (n = 10), SAH + vehicle (10% DMSO dissolved in corn oil, n = 10), SAH + AVE (0.9 mg/kg, n = 9). Rotarod test was performed on day 7, day 14, and day 21 after SAH. Morris water maze was performed on day 22–27 after SAH. The rats were euthanized on day 28 and Fluoro-Jade C staining was performed to determine the neuronal degeneration.

2.2.4. Experiment 4

To explore the mechanism of the neuroprotective role of AVE, 24 rats were randomly divided and assigned to four groups: SAH + AVE + NS (0.9% NaCl, n = 6), SAH + AVE + A779 (30 μmol/ml in 0.9% NaCl, n = 6), SAH + AVE + scr siRNA (500 pmol of scrambled siRNA, n = 6), SAH + AVE + UCP-2 siRNA (500 pmol of UCP-2 siRNA, n = 6). Ipsilateral brains were collected for Western blot analysis after neurobehavioral tests 24 h after SAH. In addition, to determine the knock-down efficiency of UCP-2 siRNA, 24 rats were subjected into four groups: naive + scr siRNA (500 pmol of scrambled siRNA, n = 6), naive + UCP-2 siRNA (500 pmol of UCP-2 siRNA, n = 6), SAH + scr siRNA (500 pmol of scrambled siRNA, n = 6), and SAH + UCP-2 siRNA (500 pmol of UCP-2 siRNA, n = 6). The expression of UCP-2 in the ipsilateral brain at 24 h after SAH were analyzed using Western blot.

2.3. SAH model

The endovascular perforation model of SAH was performed as previously described [27]. Briefly, rats were intubated and mechanically ventilated at respiratory rate of 77 throughout the operation with 2–3% isoflurane in the air (isoflurane was reduced to 1.5% at the moment of puncture). A sharp 4–0 monofilament nylon suture was inserted into the left internal carotid artery from the external carotid artery and common carotid bifurcation. The suture was advanced until the resistance was felt at the bifurcation of the anterior and middle cerebral arteries. The suture was further advanced to puncture the vessel and immediately withdraw. Rats in Sham group underwent the same procedure; however, the suture was withdrawn without puncture. The skin incision was sutured after removal of the suture. Rats were under constant monitoring intraoperatively and postoperatively. Intraoperative monitoring included peak inspiration pressure, skin pigmentation, and pedal reflex (firm toe pinch). We monitored these vitals every 5 min to ensure our animals were not in distress and were responding to the anesthesia and procedure accordingly. As the surgery lasted only 15–20 min, arterial blood gas, and blood pressure were not analyzed. Postoperatively the animals were intensely monitored while being ventilated for at least 5 min after the anesthesia was stopped. After discontinued ventilation, the animal was transferred to a heated chamber with a temperature maintained at 37.5 °C. Respiration and mucous color were monitored every 10 min until maintaining upright posture and walking normally. If the rat's respiration and behavior
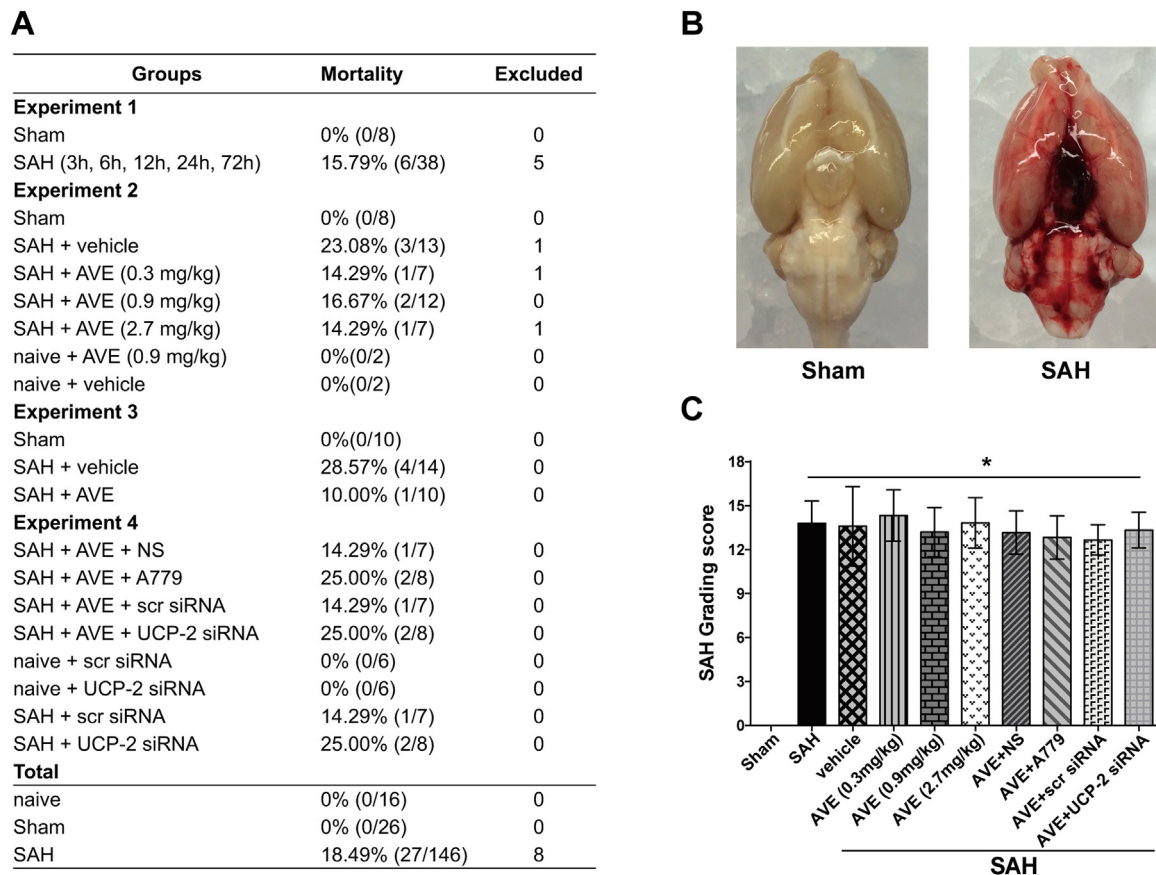
A

Groups	Mortality	Excluded
Experiment 1		
Sham	0% (0/8)	0
SAH (3h, 6h, 12h, 24h, 72h)	15.79% (6/38)	5
Experiment 2		
Sham	0% (0/8)	0
SAH + vehicle	23.08% (3/13)	1
SAH + AVE (0.3 mg/kg)	14.29% (1/7)	1
SAH + AVE (0.9 mg/kg)	16.67% (2/12)	0
SAH + AVE (2.7 mg/kg)	14.29% (1/7)	1
naive + AVE (0.9 mg/kg)	0%(0/2)	0
naive + vehicle	0%(0/2)	0
Experiment 3		
Sham	0%(0/10)	0
SAH + vehicle	28.57% (4/14)	0
SAH + AVE	10.00% (1/10)	0
Experiment 4		
SAH + AVE + NS	14.29% (1/7)	0
SAH + AVE + A779	25.00% (2/8)	0
SAH + AVE + scr siRNA	14.29% (1/7)	0
SAH + AVE + UCP-2 siRNA	25.00% (2/8)	0
naive + scr siRNA	0% (0/6)	0
naive + UCP-2 siRNA	0% (0/6)	0
SAH + scr siRNA	14.29% (1/7)	0
SAH + UCP-2 siRNA	25.00% (2/8)	0
Total		
naive	0% (0/16)	0
Sham	0% (0/26)	0
SAH	18.49% (27/146)	8

B

Sham   SAH

C

Fig. 1. **Mortality and SAH grade.** (A) Animal usage and mortality of all experiment groups. (B) Representative pictures showed that subarachnoid blood clots were mainly presented around the circle of Willis in the rat brain at 24 h post SAH. (C) SAH grade scores of all SAH groups. Data represent with mean ± SD (n = 6 per group). *$P < 0.05$ vs. Sham group. vehicle, 10% dimethyl sulfoxide (DMSO) dissolved in corn oil; AVE, AVE0991; NS, normal saline; siRNA, small interfering ribonucleic acid; scr siRNA, scrambled siRNA.

appeared normal 60 min following the procedure, then they were transferred back to their home cage and re-evaluated at days end.

2.4. Assessment of SAH grade

The SAH grade was evaluated by an investigator who was blind to the experiment through a grading system immediately after euthanasia as previously described before [28]. Briefly, the basal cistern was divided into six parts, and each part was scored from 0 to 3 according to the amount of subarachnoid blood clots present. The total score was calculated by adding all area scores (maximum SAH grade = 18). SAH rats with a score of 8 or less were excluded from this study (Fig. 1B-C).

2.5. Drug administration

2.5.1. Intranasal administration

Intranasal administration at 1 h after SAH was performed as previously described [29]. Rats were placed in a supine position under 2% isoflurane anesthesia. 10% DMSO or AVE (MedChem Express, NJ, USA) at three different dosage (0.3 mg/kg, 0.9 mg/kg, and 2.7 mg/kg) dissolved in 10% DMSO were administered intranasally. A total volume of 36 μL was administered alternately into left and right nares, 6 μL one naris every 5 min for a period of 30 min.

2.5.2. Intracerebroventricular injection

The intracerebroventricular injection was performed as previously described [30]. Rats were placed in a stereotaxic apparatus under 2.5% isoflurane anesthesia. The needle of a 10 μL Hamilton syringe (Microliter 701, Hamilton Company, USA) was inserted through a burr hole

into the right ventricle at the following coordinates relative to bregma: 1.5 mm lateral, 0.9 mm posterior, and 3.3 mm beneath the horizontal plane of the skull. Drug or siRNA was infused into ventricle at a rate of 1 μL/min by a pump, and the needle was kept in place for 5 min after the end of each injection to prevent reflux. Mas inhibitor A779 (BACHEM, CA, USA) was prepared at a concentration of 30 μmol/ml in sterile normal saline, and 5.0 μL of normal saline or A779 were infused at 1 h before SAH induction. UCP-2 siRNA or scrambled siRNA was prepared at a concentration of 100 p.m./μL in RNase free resuspension buffer. To enhance the knockdown efficiency, three different UCP-2 siRNA were mixed: (1) 5`-GGAACGUAGUAAUGUUUGUCACCTA-3`; (2) 5`-CCUCAUGACAGACGACCUCCCUUGC − 3`; (3) 5`-GCACUGUCGAA GCCUACAAGACCAT-3`. A total volume of 5.0 μL UCP-2 siRNA was injected at 48 h before SAH induction. The same volume of scrambled siRNA was used as a negative control: 5`-CGUUAAUCGCGUAUAAUA CGCGUAT-3`.

2.6. Liquid chromatography–mass spectrometry

The Liquid Chromatography–Mass Spectrometry (LC-MS/MS) system comprised an HPLC-pump, autosampler, and Agilent 6410 Triple Quadrupole LC/MS (Agilent Technologies, CA, USA) with an atmospheric pressure chemical ionization source. The brain samples were prepared as previously described [31]. Briefly, 200 mg of brain tissue was homogenized, then 2 ml of acetonitrile (Sigma-Aldrich, USA) was added. The mixture was centrifuged at 14,000 g for 30 min at 4 °C. The supernatant was transferred to a tube and dried under a negative pressure (below 2.0 kPa) for 7 h. The residue was reconstituted with 200 μL 50% acetonitrile in water (v: v). After centrifugation at 14,000 g

for 20 min at 4 ℃, 20 μL of the supernatant was injected into the LC-MS/MS system. MS spectra were collected in positive reflector mode from m/z 100–700. MS/MS spectra were acquired using a collision energy of 34 kV with the metastable suppressor on. MassHunter Software Version B.08.00 (Agilent Technologies, CA, USA) was used for the visualization and analysis of the LC-MS/MS data.

2.7. Short-term neurological performance evaluation

The short-term neurological performance was evaluated at 24 h after SAH in a blinded fashion with modified Garcia scale and beam balance test as previously described [30]. Modified Garcia scale includes judgments of spontaneous activity $(0 - 3)$, symmetry in the movement of four limbs $(0 - 3)$, forepaw outstretching $(0 - 3)$, climbing $(1 - 3)$, body proprioception $(1 - 3)$, and response to vibrissae touch $(1 - 3)$. The rats were also placed on a beam, and the walking distance within 1 min was measured for the beam balance test $(0 - 4)$.

2.8. Long-term neurological performance evaluation

2.8.1. Rotarod test

The rotarod test was performed on day 7, 14, and 21 after SAH to evaluate sensorimotor coordination as previously described [32]. The rotating speed was started at 5 revolutions per minute (RPM) and 10 RPM respectively and was gradually increased by 2 RPM every 5 s. The duration that rats were able to stay on the accelerating rotating cylinder was recorded by a photo beam circuit.

2.8.2. Morris Water Maze

Water maze test was started on day 22–27 after SAH to evaluate spatial learning capacity and reference memory as previously showed [33]. The cued water maze test was performed on day 22 after SAH, which was used as a control to assess any sensorimotor and/or motivational deficits that could affect performance during the spatial water maze test. The spatial water maze test was performed on day 23–26 after SAH. On day 27, the animals were tested with a 60-sec probe trial in which the platform was removed from the water. A video recording system traced the activities of the animals and the swim patterns were measured for quantification of distance, latency, and swimming speed by Video Tracking System SMART-2000 (San Diego Instruments Inc., CA, USA).

2.9. Histological analysis

Rats were deeply anesthetized and transcardially perfused with 100 ml of chilled phosphate buffered saline (PBS, 0.01 M, pH 7.4) followed by 100 ml of 4% paraformaldehyde (PFA). The whole brains were rapidly collected and fixed in 4% PFA at 4 ℃ for 24 h, followed in 30% sucrose solution for 72 h. After being embedded into OCT compound (Scigen Scientific Gardena, CA, USA) and frozen at − 80 ℃, 8 μm coronal brain sections were cut on a cryostat (LM3050S, Leica Microsystems, Bannockburn, Germany) for double immunofluorescence [30], TUNEL [34], Fluoro-Jade C [35], and DHE staining [36]. The slides were observed and photographed under a fluorescence microscope (DMi8, Leica Microsystems, Germany).

2.9.1. Immunofluorescence staining

Slides were washed with 0.01 M of PBS three times for 5 min then incubated in 0.3% Triton X-100 in 0.01 M of PBS for 5 min at room temperature. After being blocked with 5% donkey serum in 0.01 M of PBS for 1 h at room temperature, the sections were incubated at 4 ℃ overnight with primary antibody including: anti-Mas (1:200, NBP178444, NOVUS, CO, USA), anti-NeuN (1:500, ab177487, Abcam, Cambridge, MA, USA). Then, the sections were washed with 0.01 M of PBS and incubated with fluorescence-conjugated secondary antibodies (1:500, Jackson ImmunoResearch, PA, USA) for 1 h at room

temperature.

2.9.2. TUNEL staining

For quantification of neuronal apoptosis, double staining of neuron marker NeuN and terminal deoxynucleotidyl transferase dUTP nick end labeling (TUNEL) staining was performed using in situ Apoptosis Detection Kit (Roche, USA) according to the manufacturer's instructions at 24 h after SAH. The number of TUNEL-positive neurons was counted manually in the ipsilateral cortex. Six sections per brain over a microscopic field of 20x were averaged. Data were presented as the ratio of TUNEL-positive neurons (%).

2.9.3. Fluoro-Jade C staining

Fluoro-Jade C (FJC) staining was performed using Fluoro-Jade C Ready-to-Dilute Staining Kit (Biosensis, USA) for identifying degenerating neurons according to the manufacturer's instructions. FJC-positive neurons were counted in six sections per brain with ImageJ software (ImageJ 1.5, NIH, USA) to evaluate the extent of the neuronal damage. The data were presented with the average number of FJC-positive neurons in the fields as cells/mm^2.

2.9.4. DHE staining

To assess the brain oxidative stress level, freshly prepared frozen brain sections were incubated with 2 μmol/L fluorescent dye dihydroethidium (DHE, Thermo Fisher Scientific, USA) at 37 ℃ for 30 min in a humidified chamber and protected from light. Digital images were captured and the red fluorescence intensity was quantified by using NIH ImageJ software. The fluorescence intensity was expressed relative to that of Sham rats.

2.10. Western blot analysis

Western blot was performed as previously described [37]. Rats were anesthetized with isoflurane at 24 h after SAH and transcardially perfused with 100 ml of chilled PBS (0.01 M, pH7.4) before brains collection to ensure that there were no blood contaminants. The left hemispheres were instantly collected and snap frozen in liquid nitrogen, then placed in − 80 ℃ for storage until use. Brain samples were homogenized in RIPA lysis buffer (sc-24948, Santa Cruz Biotechnology Inc., TX, USA) and further centrifuged at 14,000 g at 4 ℃ for 30 min. Equal amounts of protein (30 μg) were loaded onto 7.5% − 12.5% SDS-PAGE gel, then electrophoresed and transferred to nitrocellulose membranes (0.2 μm), which were blocked with 5% non-fat blocking grade milk (Bio-Rad, Hercules, CA, USA) and incubated with the following primary antibodies overnight at 4 ℃: anti-Mas (1:2000, NBP178444, NOVUS Biologicals, CO, USA), anti-PKA-Cα (1:3000, 4782, Cell Signaling Technology Inc., MA, USA), anti-p-CREB (1:1000, 9198, Cell Signaling Technology Inc., MA, USA), anti-CREB (1:1000, 9197, Cell Signaling Technology Inc., MA, USA), anti-UCP-2 (1:2000, 89326, Cell Signaling Technology Inc., MA, USA), anti-Bcl-2 (1:2000, ab59348, Abcam, MA, USA), anti-Bax (1:4000, ab182734, Abcam, MA, USA), anti-Romo-1 (1:200, AVIVA Systems Biology, CA, USA), and anti-β-actin (1:4000, sc-47778, Santa Cruz Biotechnology Inc., TX, USA). On the following day, the membranes were incubated with the appropriate secondary antibody (1:4000, Santa Cruz Biotechnology Inc., TX, USA) at room temperature for 1 h. Immunoblots were then visualized with ECL Plus chemiluminescence reagent kit (Amersham Bioscience, PA, USA) and quantified with optical methods using the ImageJ software (ImageJ 1.5, NIH, USA). The results were normalized using β-actin as an internal control.

2.11. Statistical analysis

Data were presented as the mean ± standard deviation (SD) and analyzed using GraphPad Prism 7 (La Jolla, CA, USA). Statistical evaluation of the data was performed by analysis of variance (ANOVA),
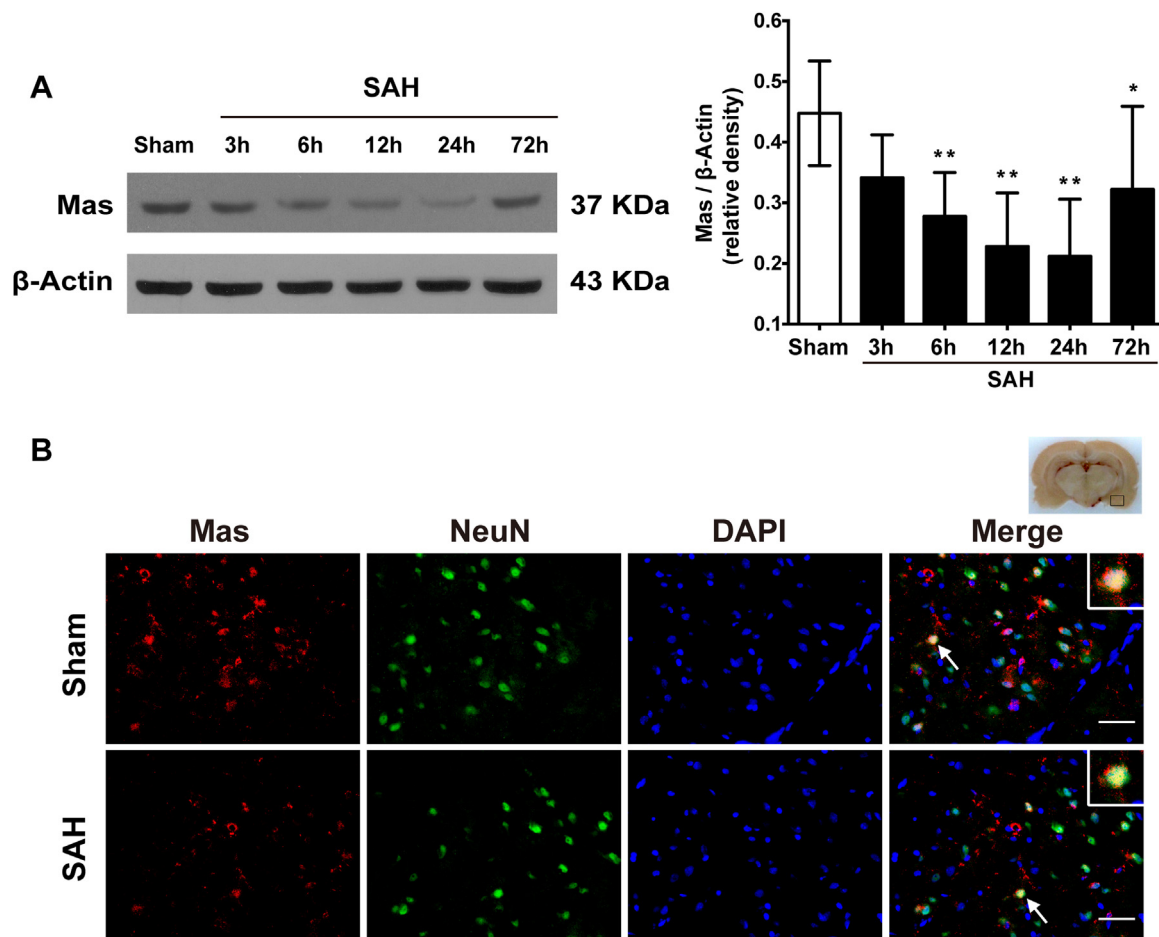
Fig. 2. Temporal expression of Mas in the brain after subarachnoid hemorrhage (SAH). (A) Representative Western blot image and quantitative analysis of Mas from the ipsilateral hemisphere in time course experiment after SAH. Data represent with mean ± SD (n = 6 per group). *$P < 0.05$, **$P < 0.01$ vs. Sham group. (B) Representative microphotographs of double immunofluorescence staining showed that Mas (red) co-localized with NeuN-positive neurons (green) in both Sham and SAH groups (n = 2 per group). Top panel indicates the location of staining (small black box). Scale bar = 50 μm.

followed by Tukey multiple-comparison post hoc analysis. A p-value < 0.05 was considered statistically significant.

3. Results

3.1. Mortality and SAH severity

Of the total 196 animals used, 146 were subjected into SAH induction, of which 27 (18.49%) rats died within 24 h after SAH. 8 rats were excluded from the study due to mild SAH. No rat died in Sham and naive groups (Fig. 1A). After SAH, blood clots were present around the circle of Willis with a significant difference in SAH grade between Sham and SAH animals, but no significant difference was observed between all SAH groups at 24 h after SAH (Fig. 1B-C).

3.2. Expression changes of Mas in ipsilateral hemisphere at 24 h after SAH

Western blot results showed that expression of Mas dramatically decreased after SAH induction and reached to the lowest level at 24 h when compared to Sham group (Fig. 2A). Double immunofluorescence staining showed that Mas was mainly expressed in neurons in the brain, and the number of Mas-positive neurons was decreased in SAH (24 h) group when compared with that in Sham group (Fig. 2B).

3.3. Determination of AVE in brain after intranasal administration

AVE in the brain after a single intranasal dose was measured using

LC-MS/MS. The full scan MS signal of AVE detected from the AVE standard (Fig. s2A) showed characteristic peak at *m/z* 581. MS/MS spectra of precursor ion at *m/z* 581 from AVE in the brain of dosed rats showed similar ion pattern as that observed from AVE standard (Fig. s2B-C), indicating that AVE could penetrate into brain by intranasal administration.

3.4. AVE improved short-term neurological functions at 24 h after SAH

Significant neurological impairments were observed in SAH + vehicle group at 24 h after SAH when compared with Sham group as assessed by modified Garcia scale and beam balance test. AVE treatment at middle dose (0.9 mg/kg) significantly improved neurological performance (both modified Garcia score and beam balance score) at 24 h after SAH (Fig. 3A-B); however, low dose (0.3 mg/kg) or high dose (2.7 mg/kg) only improved modified Garcia score, but not the beam balance score at 24 h after SAH (Fig. 3B). Based on this finding, AVE at a dose of 0.9 mg/kg was used in the subsequent studies.

3.5. AVE reduced neuronal apoptosis at 24 h after SAH

As SAH results in neuronal apoptosis, TUNEL staining was used to see whether AVE can reduce this kind of injury at 24 h after SAH. The TUNEL-positive neurons of the ipsilateral cortex in SAH + vehicle group increased significantly compared with Sham group at 24 h after SAH, but the treatment of AVE could reduce the number of TUNEL-positive neurons (Fig. 3C). Western blot data showed that Bax was significantly
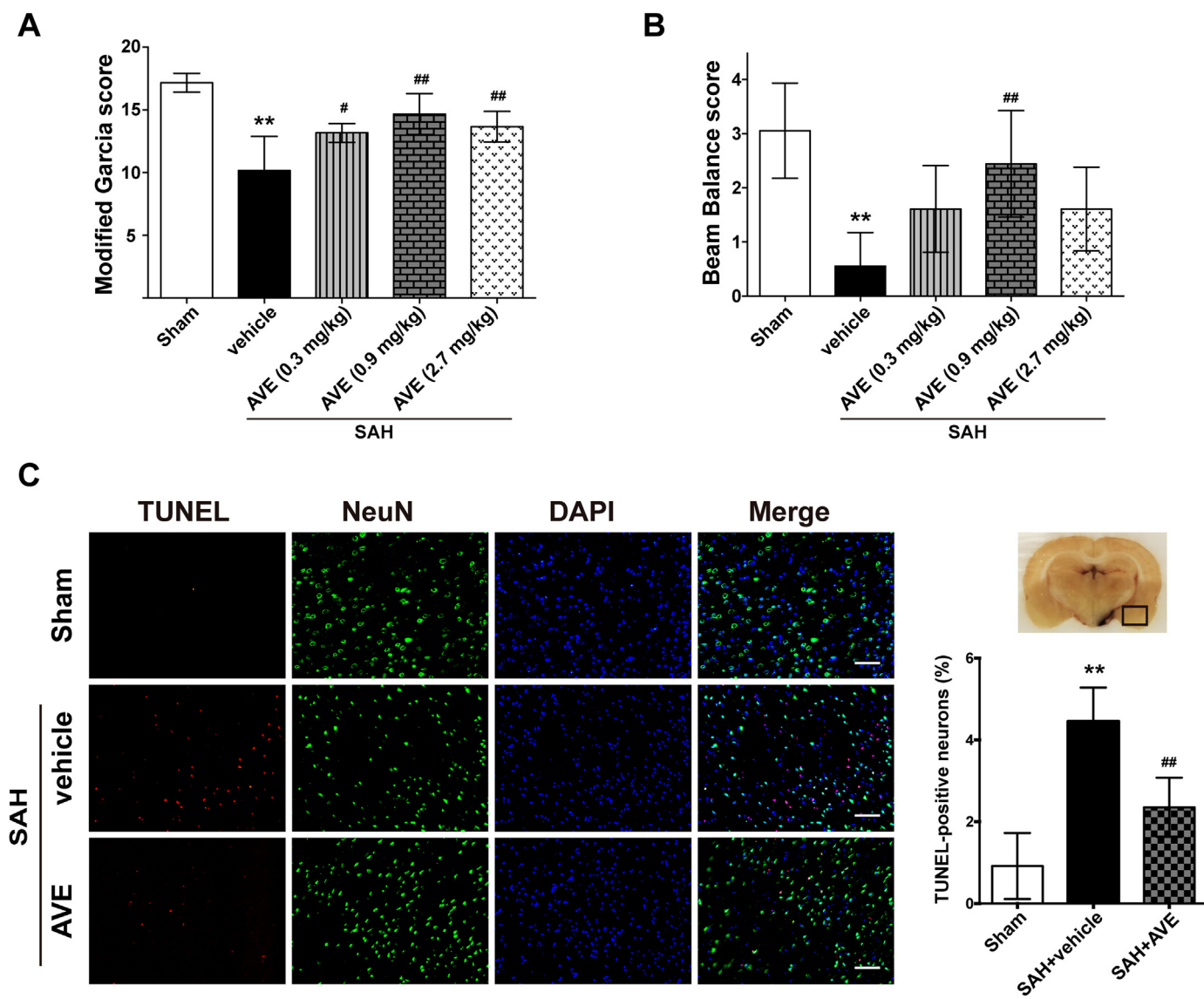
Fig. 3. Effects of AVE 0991 on short-term (24 h) neurological function and neuronal apoptosis after subarachnoid hemorrhage (SAH). Neurological scores assessed with (A) modified Garcia scale and (B) beam balance test at 24 h after SAH. Data represent with mean ± SD (n = 6 per group). (C) Representative microphotographs and quantitative analysis of TUNEL-positive neurons in the ipsilateral cortex 24 h after SAH. Top panel indicates the location of staining (small black box). Data represent with mean ± SD (n = 4 per group). $**P < 0.01$ vs. Sham group; $^{\#}P < 0.05$, $^{\#\#}P < 0.01$ vs. SAH + vehicle group. vehicle, 10% DMSO dissolved in corn oil; AVE, AVE 0991. Scale bar = 100 μm.

increased and Bcl-2 was significantly decreased after SAH, and AVE treatment could reduce the expression of Bax and induce the expression of Bcl-2 (Fig. 8C-D).

3.6. AVE reduced the oxidative stress injury of the ipsilateral hemisphere at 24 h after SAH

Oxidative stress level of ipsilateral *hemisphere* after SAH was measured by DHE staining as well as the expression of Romo-1 by Western blot. The intensity of DHE in SAH + vehicle group was evident compared with Sham group at 24 h after SAH (Fig. 4A-B). Intranasal administration with AVE could significantly reduce the intensity of DHE when compared with the group of SAH + vehicle (Fig. 4A-B). Our data showed that Romo-1, a marker of oxidative stress [38], was remarkably increased at 24 h after SAH compared with Sham group (Fig. 4C), and the treatment with AVE could significant reduce the level of Romo-1 (Fig. 4C).

3.7. AVE improved long-term neurological functions at four weeks after SAH

SAH resulted in persistent neurologic deficits in rotarod performance over the 3-week period. AVE treatment significantly improved sensorimotor coordination 1 week after SAH at both 5 RPM and 10 RPM acceleration compared to SAH + vehicle group. However, no significant difference of latency in rotarod test between SAH + AVE and SAH + vehicle group was observed at week 2 or 3 after SAH (Fig. 5A). In addition, the learning task revealed prolonged escape latencies (Fig. 5B, left panel), longer swimming distances (Fig. 5B, right panel), and less time spent in probe quadrant (Fig. 5C-D) in SAH + vehicle group when compared with Sham group. AVE-treated group showed significant memory recovery compared with SAH + vehicle group in reduced escape latency, reduced swimming distance to platform, and spent more time in target quadrant (Fig. 5B-D). No significant difference was observed in swimming speed between groups (Fig. 5E).
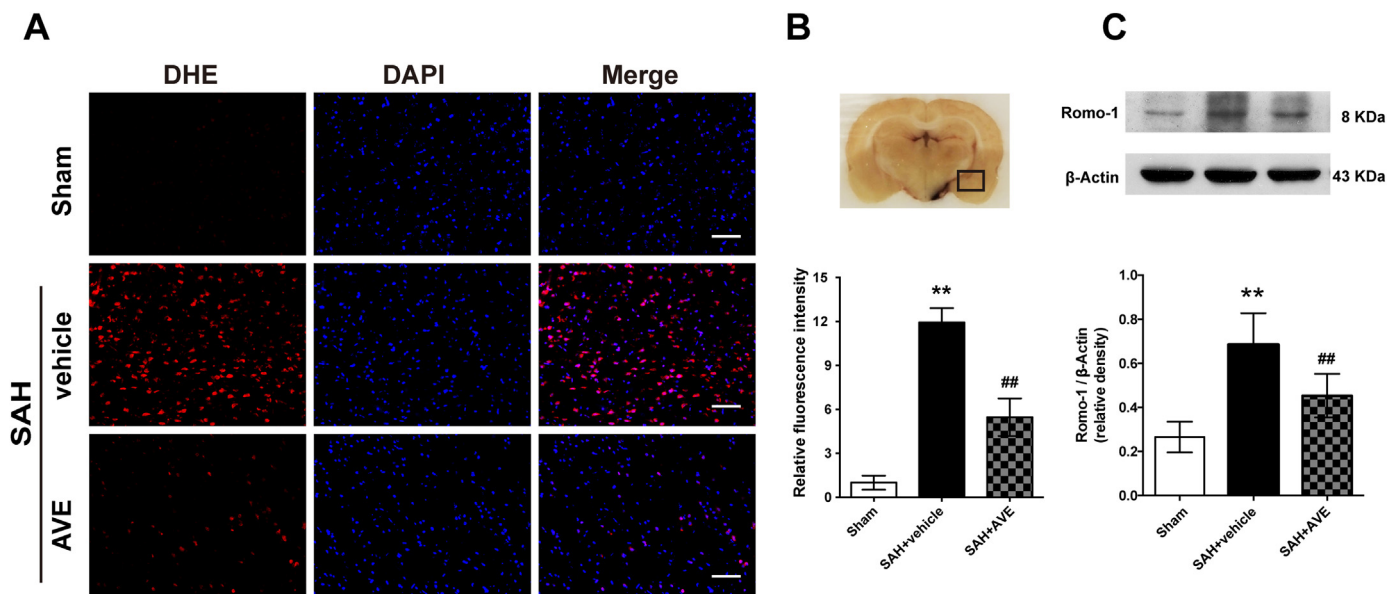
Fig. 4. Effects of AVE 0991 on oxidative stress level of ipsilateral cortex in rat brain at 24 h after subarachnoid hemorrhage (SAH). (A) Representative microphotographs of DHE staining in the ipsilateral cortex of rat brain. (B) Quantitative analysis of DHE fluorescence intensity (n = 4 per group). Top panel indicates the location of staining (small black box). (C) Representative Western blot image and quantitative analysis of Romo-1 expression (n = 6 per group). $**P < 0.01$ vs. Sham group; $^{\#\#}P < 0.01$ vs. SAH + vehicle group. vehicle, 10% DMSO dissolved in corn oil; AVE, AVE 0991. Scale bar = 100 μm.

3.8. AVE reduced hippocampal neuronal degeneration at 28 d after SAH

As known, the hippocampus plays an important role in memory formation [39], Floro-Jade C staining was used to see whether AVE can attenuate neuronal degeneration in different regions of ipsilateral hippocampus. Robust Floro-Jade C staining in CA1, CA2, and DG of ipsilateral hippocampus were observed at 28 d after SAH. However, AVE treatment significantly reduced the number of Floro-Jade C-positive neurons in ipsilateral hippocampus when compared to SAH + vehicle group (Fig. 6).
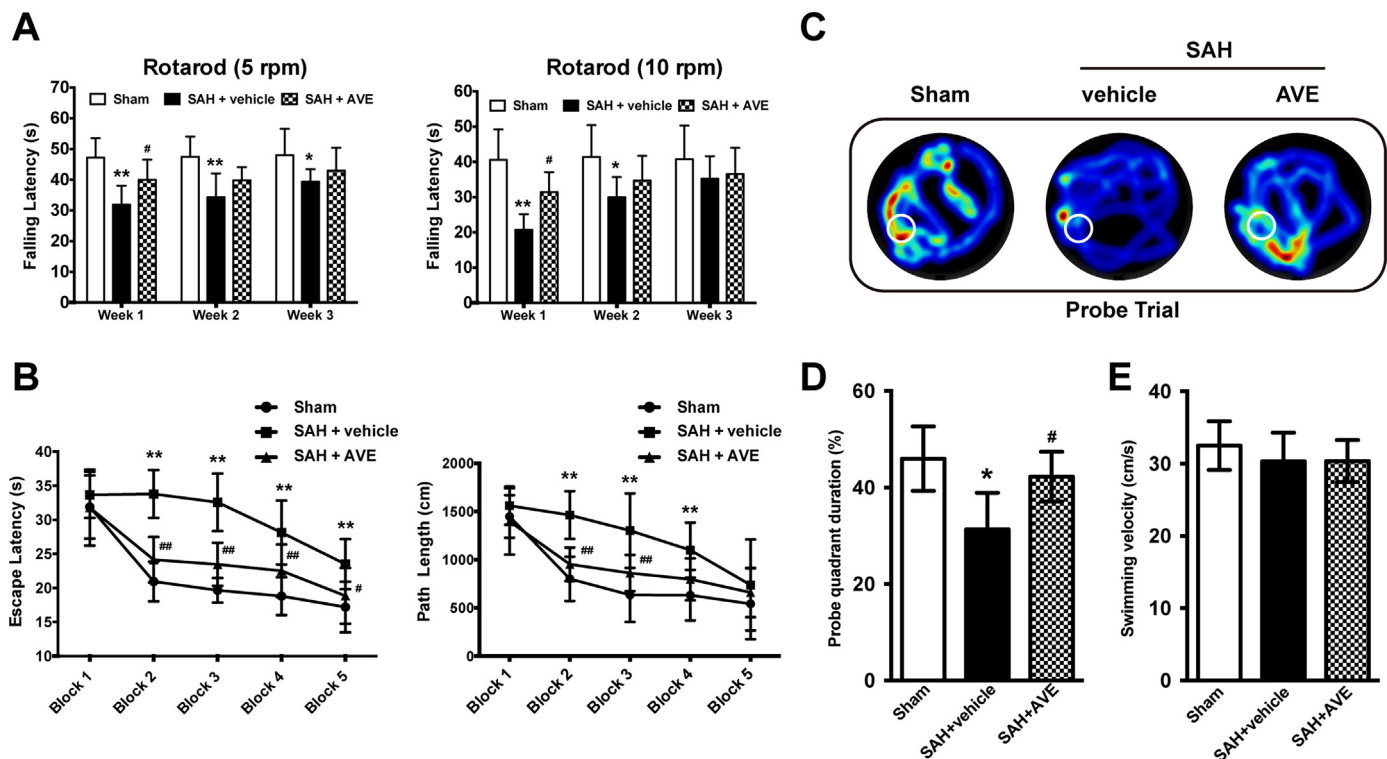

Fig. 5. Effect of AVE 0991 on long-term neurological function at 28 d after subarachnoid hemorrhage (SAH). (A) Rotarod tests of 5 RPM and 10 RPM. (B) Escape latency and swimming distance of Morris Water Maze. (C) Representative heatmaps of the probe trial. The white circles indicate the positions of the probe platform. (D) Quantification of the probe quadrant duration in the probe trial. (E) Swimming velocities of different groups in probe trial. Data represent with mean ± SD (n = 9–10 per group). $*P < 0.05$, $**P < 0.01$ vs. Sham group; $^{\#}P < 0.05$, $^{\#\#}P < 0.01$ vs. SAH + vehicle group. vehicle, 10% DMSO dissolved in corn oil; AVE, AVE 0991.
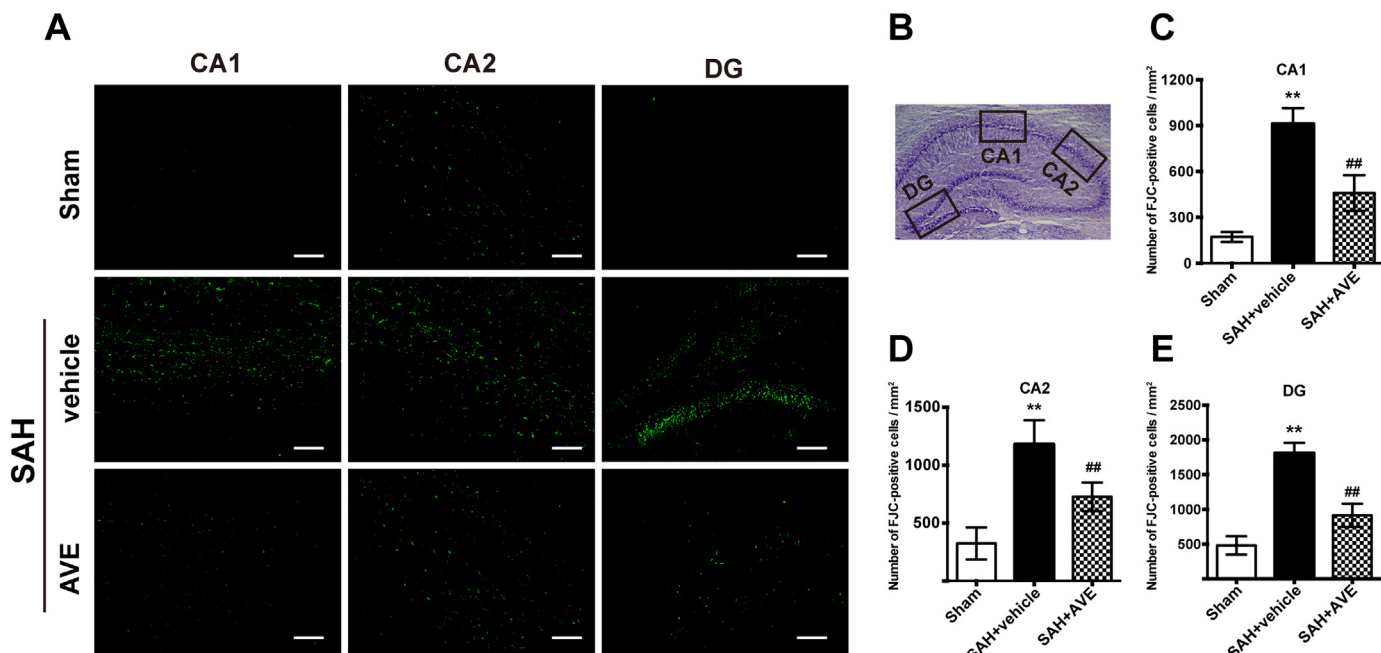
Fig. 6. Effect of AVE on neuronal degeneration at 28 d after subarachnoid hemorrhage (SAH). (A) Representative Fluoro-Jade C staining pictures in different regions of hippocampus (CA1, CA2, and DG) at 28 d after SAH. (B) Regions of interest areas in the ipsilateral hippocampus. Quantification of the Fluoro-Jade C-positive cells in (C) CA1, (D) CA2, and (E) DG. Data represent with mean ± SD (n = 4 per group). $* * P < 0.01$ vs. Sham group; $^{\#\#}P < 0.01$ vs. SAH + vehicle group. vehicle, 10% DMSO dissolved in corn oil; AVE, AVE 0991. Scale bars of CA1 and CA2 = 100 μm; Scale bar of DG = 200 μm.

3.9. A779 and UCP-2 siRNA blunt the protective effects of AVE on short-term neurologic functions at 24 h after SAH

The knockdown efficacy of UCP-2 siRNA was demonstrated by Western blot in both naive and SAH animals. UCP-2 siRNA administered by i.c.v injection significantly decreased UCP-2 expression in the ipsilateral hemisphere in both naive and SAH rats (Fig. 7A). Consistently, UCP-2 in vivo knockdown aggravated SAH-induced neurologic deficits (Fig. 7B-C) and markedly reversed the beneficial effects of AVE in SAH + AVE + UCP2-siRNA group when compared to SAH + AVE + scr siRNA group (Fig. 8A-B). Administration of A779 significantly decreased the neurological scores of modified Garcia and beam balance in SAH + AVE + A779 group when compared to SAH + AVE + NS group (Fig. 8A-B).

3.10. AVE suppressed apoptosis via activation of Mas/PKA/CREB/UCP-2 signaling pathway at 24 h after SAH

Western blot data showed that SAH significantly increased the expression of PKA-Cα, p-CREB, UCP-2, Bax, and Romo-1 at 24 h after SAH when compared to Sham group. Moreover, the expression of Bcl-2 remarkably decreased at 24 h after SAH when compared to Sham group (Fig. 8C-D). AVE treatment further increased the expression of PKA-Cα, p-CREB, UCP-2, and Bcl-2, but the expression of Bax and Romo-1 were decreased in SAH + AVE group when compared with SAH + vehicle group. Mas inhibitor A779 was administered 1 h before SAH induction to assess Mas involvement in the anti-apoptotic pathway of AVE in SAH model. Our data showed that pretreatment with A779 significantly decrease the downstream molecule PKA-Cα, as well as p-CREB, UCP-2
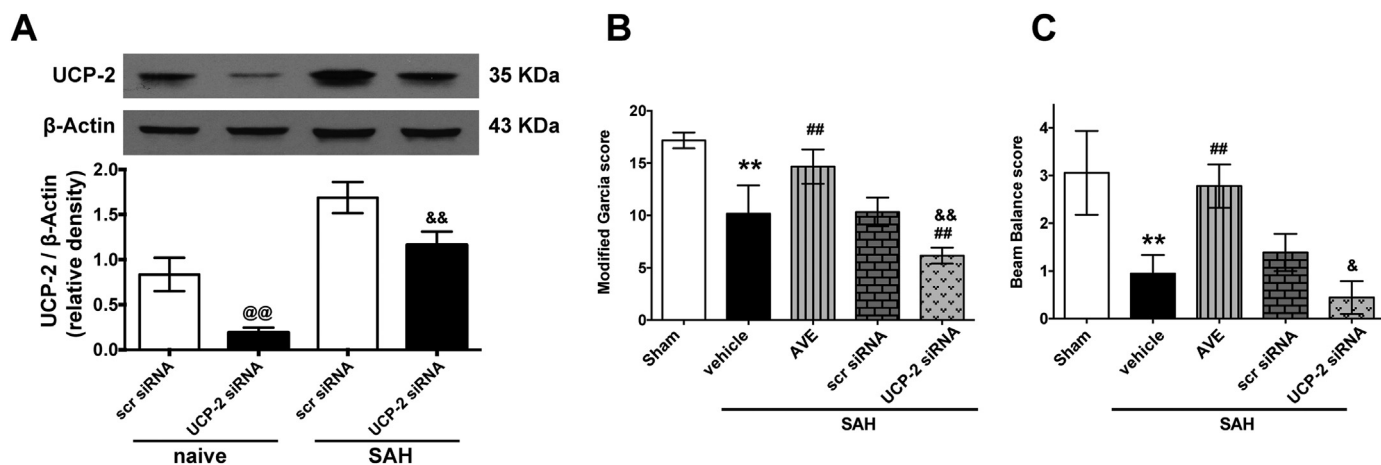

Fig. 7. Effects of UCP-2 knock down on neurological function at 24 h after subarachnoid hemorrhage (SAH). (A) Expression of UCP-2 after administration of UCP-2 siRNA by intracerebroventricular injection in naive and SAH rats. (B-C) The neurological functions of SAH groups after administration of UCP-2 siRNA. Data represent with mean ± SD (n = 6 per group). $^{@@}P < 0.01$ vs. naive + scr siRNA group; $^{\&}P < 0.05$, $^{\&\&}P < 0.01$ vs. SAH + scr siRNA group; $* * P < 0.01$ vs. Sham group; $^{\#\#}P < 0.01$ vs. SAH + vehicle group; vehicle, 10% DMSO dissolved in corn oil; AVE, AVE 0991; siRNA, small interfering ribonucleic acid; scr siRNA, scrambled siRNA.
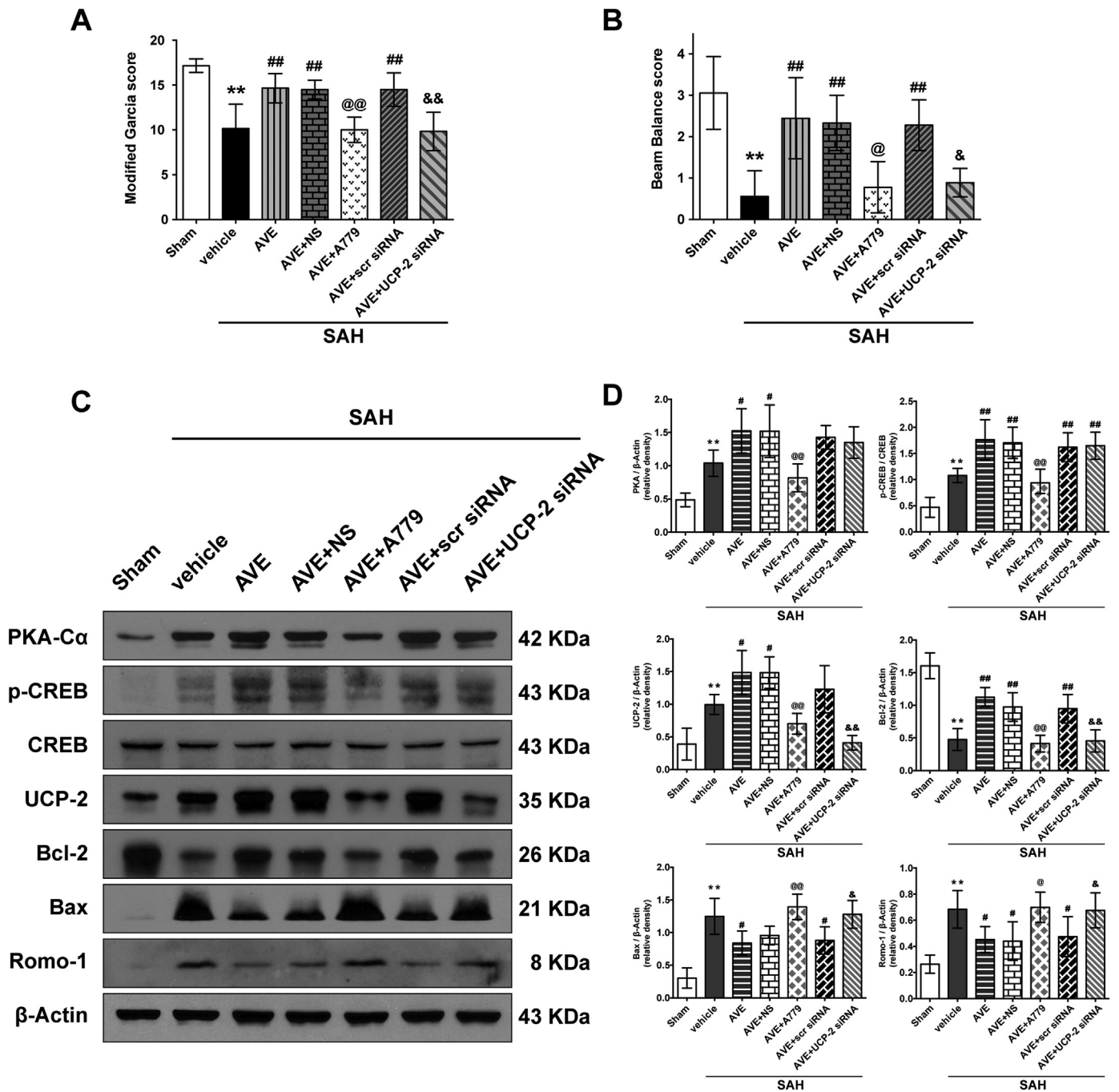
Fig. 8. Inhibition of Mas or knockdown of UCP-2 abolished the anti-apoptotic effect of AVE at 24 h after subarachnoid hemorrhage (SAH). (A) Modified Garcia score. (B) Beam balance score. (C-D) Representative Western blot images and quantification of and PKA-Cα, p-CREB, CREB, UCP-2, Bcl-2, Bax, and Romo-1. Data represent with mean ± SD (n = 6 per group). $**P < 0.01$ vs. Sham group; $^{\#}P < 0.05$, $^{\#\#}P < 0.01$ vs. SAH+vehicle group; $^{@}P < 0.05$, $^{@@}P < 0.01$ vs. SAH+AVE+NS group; $^{\&}P < 0.05$, $^{\&\&}P < 0.01$ vs. SAH+AVE+scr siRNA group. vehicle, 10% DMSO dissolved in corn oil; AVE, AVE0991; NS, normal saline; siRNA, small interfering ribonucleic acid; scr siRNA, scrambled siRNA.

and Bcl-2 in SAH + AVE + A779 group when compared to SAH + AVE + NS group. Consistently, significant overexpression of Bax and Romo-1 were observed in SAH + AVE + A779 group when compared to SAH + AVE + NS group. UCP-2 knockdown by i.c.v injection of UCP-2 siRNA 48 h before the induction of SAH evidently suppressed the expression of UCP-2 at 24 h after SAH in SAH + AVE + UCP-2 siRNA group when compared to SAH + AVE + scr siRNA group. Moreover, silence of UCP-2 sufficiently decreased the Bcl-2 expression, while increase the Bax and Romo-1 expression in SAH + AVE + UCP-2 siRNA group, when compared with that in SAH + AVE + scr siRNA group. UCP-2 silence did not change the express of PKA-Cα and phosphorylation of CREB (Fig. 8C-

D).

4. Discussion

In this present study, we assessed the neuroprotective effects of AVE and explored the underlying mechanism of AVE in oxidative stress and neuronal apoptosis during EBI after SAH. The major novel findings of this study are: (1) Mas axis of brain RAS was significantly suppressed in ipsilateral brain at 24 h after SAH in rats; (2) Intranasal administration with AVE at a dose of 0.9 mg/kg remarkably reduced oxidative stress and neuronal apoptosis in EBI at 24 h after SAH, which was

accompanied by the improvement of neurological dysfunction. (3) AVE treatment was associated with upregulation of PKA-Cα, p-CREB, UCP-2, and Bcl-2 and downregulation of Bax and Romo-1 in the brain at 24 h after SAH in rats. (4) Blockage of Mas or silence of UCP-2 partially offset the beneficial effects of AVE on neurological functions and expression of apoptotic markers. Our data, collectively, suggests that the neuroprotective action of AVE in EBI after SAH involves Mas/PKA/CREB/UCP-2 signaling pathway.

Accumulating scientific evidence suggested that neuronal apoptosis is one of the major pathological processes involved in neurological impairment in EBI after SAH [2]. Neuronal apoptosis has been shown to occur in the brain cortex as well as hippocampus which were associated with oxidative stress injury following SAH [5]. Mitochondrial uncoupling has been proposed as an important mechanism to reduce mitochondrial ROS levels and attenuate cell death [40,41]. Mitochondrial uncoupling mediated by UCP-2 in neurons has been suggested to prevent neuronal apoptosis in traumatic brain injury and ischemic stroke models [12]. Another study found that the expression of UCP-2 was associated with the phosphorylation level of CREB, which also has been suggested to be the downstream signal of the Mas receptor [42]. However, the mechanism between mitochondrial uncoupling and Mas have not been elucidated in SAH. In the present study, we for the first time, demonstrated that intranasal administration of AVE can enhance mitochondrial uncoupling and reduce oxidative stress injury and neuronal apoptosis in a Mas dependent manner.

Mas is a G-protein coupled receptor and has been identified as one of the major components of RAS, which holds promise as a potential target for stroke therapies [43,44]. It is widely expressed in different organs, but with the highest level in the brain and testis [16]. In the brains of rats and mice, Mas transcripts are localized in the hippocampus, cerebral cortex, olfactory tubercle, piriform cortex, and olfactory bulb, and also at a lower level in the entirety of the neocortex and especially in the frontal lobe [16]. Our present data showed that Mas immunoreactivity was primarily associated with neurons, and also it can express in endothelial cells, and microglia/macrophages (data not shown) in the brain, which was consistent with previous study [18]. Mas upregulation within 48 h was first reported previously in a rat model of permanent middle cerebral artery occlusion (MCAO) [45]; however, the other two studies showed slightly different findings with downregulation in Mas at 24 h following transient MCAO model [46] and endothelin-1 induced MCAO model [19]. In our study, we found that the Mas expression in left hemisphere of brain was decreased and reached to the lowest level at 24 h after SAH. According to previous studies [47–49], the EBI was much worse at 24 h when compared with other time points after experimental SAH, of which the damaging factors may include neuronal apoptosis, brain edema, and inflammation. As Mas is primarily produced in neurons, the expression of Mas was the lowest at 24 h after SAH, corresponding to the severity of EBI. The increase of Mas expression at 72 h may be associated with a less EBI severity at later time point after SAH. It is likely that the differences in stroke models play a distinctive role in the induction of Mas expression. Taken together, current results indicate that the Mas suppressed by deleterious stress in EBI at 24 h after SAH.

AVE has a molecular weight of 580.73 and is soluble in alkaline water solutions or organic solvents (DMSO, ethanol) [22]. Previous studies have shown that it is physiologically well tolerated by systemic administration [25,50]. To keep away from its systemic effects, we delivered the drug intranasally. In our mass spectrometry study, we got similar MS/MS spectra from the brain of AVE-treated rats when compared with that from AVE standard, which means that the drug can penetrate into the brain by intranasal administration. In the current study, we administered three doses of AVE intranasally 1 h after SAH and measured the neurological functions at 24 h after SAH. Although three doses all showed significant improvements in modified Garcia test, only the medium dose can improve neurological functions as assessed by modified Garcia and beam balance test. Therefore, the

medium dose of AVE was chosen for subsequent experiments.

Although the mechanisms by which activation of Mas exerts its protective role are not clear, several studies have focused on the modulation of oxidative stress. In keeping with our results, Jiang et al. [51] demonstrated that Mas activation attenuated oxidative stress by decreasing lipid peroxidation and increasing superoxide dismutase activity in the brain of hypertensive rat. In addition, Zhang et al. [52] found that upregulation of the ACE2-Ang-(1-7)-Mas axis by genetic overexpression or pharmacological activation preserved endothelial function through normalizing overproduction of reactive oxygen species in diabetic *db/db* mice. On the contrary, a reduction in superoxide dismutase and catalase activity was observed in Mas-deficient mice demonstrating impaired antioxidant properties in these animals [53]. Taken together, these data suggested a strong causative link between enhancement of Mas and antioxidant function.

In this current study, we found that there were significant increases in the intensity of DHE staining and the numbers of TUNEL-positive neurons in ipsilateral brain cortex at 24 h after SAH. Our data showed AVE treatment can significantly reduce oxidative stress and neuronal apoptosis as measured by DHE and TUNEL staining. Also in the Western blot data, oxidative stress marker Romo-1 and pro-apoptotic marker Bax were significantly reduced while anti-apoptotic marker Bcl-2 was increased in AVE-treated group. When selective Mas inhibitor A779 was administered, it reversed the protective effect of AVE against oxidative stress and neuronal apoptosis, confirming the protective role of Mas in EBI after SAH.

Hippocampus injury in animal models of ischemia has been shown to cause long-term cognitive impairments [39,54]. Interestingly, our study showed that neurodegenerations of CA1, CA2, and DG of the hippocampus were evident even 28 d after SAH as measured in Fluoro-Jade C staining. The previous study found that activation of Mas with Ang-(1−7) can enhance long-term potential (LTP) in the hippocampus, while the antagonist A779 or Mas deletion can blunt the LTP-promoting effect of Ang-(1−7) [55]. In agreement with these observations, we found AVE treatment can significantly reduce the neuronal degeneration as measured by Floro-Jade C staining in CA1, CA2, and DG regions of the hippocampus, which was accompanied with improvement of spatial learning and memory.

Stimulatory effects of Mas on protein kinase A (PKA) activity have been documented in another study through Gs/cAMP-dependent pathway [56]. The PKA holoenzyme is inactive under basal conditions, but an increase in cAMP unleash PKA-Cα, which then catalyzes substrate phosphorylation [57]. Activated PKA can transfer the phosphate groups onto Ser/Thr residues of target proteins [58]. cAMP response element binding (CREB) protein was initially identified as a transcription factor that can be phosphorylated by PKA [58]. It is well established that CREB plays an important role in neuronal development, synaptic plasticity, memory function, regeneration, and cell survival in response to various stresses [58]. During post-ischemic recirculation, PKA activity and CREB phosphorylation in the ischemic core are rapidly suppressed after their initial transient activation, and neuronal death eventually takes place in this region [59]. By contrast, PKA in the peri-ischemic area is continuously activated with persistent phosphorylation of CREB, and neurons in this area are spared ischemic damage and survive [59]. In SAH patient, initial bleeding can cause a global ischemic impact by reducing cerebral blood flow through elevation of intracranial pressure and mechanically blocking arteries [4]. In this study, expression of PKA-Cα and phosphorylation of CREB were used to measure the PKA activity. Our data showed that phosphorylation of CREB increases at 24 h after SAH induction. We also have shown that activation of Mas with AVE increases the level of PKA-Cα the phosphorylation of CREB in the brain at 24 h after SAH, which was accompanied by improvement of neurological functions and inhibition of oxidative stress and neuronal apoptosis. These results indicate that PKA-Cα and CREB increases by compensatory mechanism after SAH and lack of this mechanism reached to neuroprotective level by AVE

treatment in SAH rats.

UCP-2 is a mitochondrial inner membrane protein that may regulate mitochondrial energy metabolism and ROS generation [12]. The previous studies found that UCP-2 is an endogenous inducible protein that can reduce brain damage by alteration of ROS release and inhibition of apoptosis after experimental stroke and brain trauma [60–62]. It was suggested that compounds inducing UCP-2 expression or activity would be neuroprotective and would preserve brain function after stroke, epilepsy or neurodegenerative disease [12,62,63]. Numerous physiological and pathological factors lead to increase expression of UCP-2 mRNA, including brain ischemia, fast, high-fat diets, suckling of newborn pups, sepsis, acute endurance exercise, and neurodegenerative disease [12]. To date, limited information is available on the regulation of UCP-2 expression. CREB and PPARγ were proposed as the transcriptional regulators in the previous study [12,58]. However, we only focus on CREB in this study as it can be phosphorylated by PKA [64]. Our results showed that the activation of Mas with AVE after SAH significantly enhanced the activity of PKA and phosphorylation of CREB, which was accompanied by an increase in UCP-2 level. While, the inhibition of Mas with A779 decrease the PKA activity and its downstream factors, such as p-CREB, UCP-2, and Bcl-2, and enhanced the expression of Bax and Romo-1. The knockdown of UCP-2 had no effect on the expression of PKA-Cα and phosphorylation of CREB, but significantly decreased the Bcl-2 expression and increased the expression of Bax and Romo-1. The results in our work reveal an important regulatory role of AVE on the UCP-2 expression in the brain after SAH. Our data also provides a functional link between UCP-2 and neuronal apoptosis after SAH. To this end, the current results shed new light on the role of AVE in reducing oxidative stress and neuronal apoptosis after SAH by stimulating the UCP-2 expression through a Mas/PKA/CREB pathway.

There are some limitations to this study. First, since it was reported that activation of Mas could protect endothelial cells and attenuate expression of inflammatory genes, so we cannot exclude the possibility that activation of Mas may also have exerted other neuroprotective effects, such as anti-inflammation and blood-brain barrier protection. Second, PPARγ was reported as one of the transcript factors of UCP-2 in other studies, however, we only focus the CREB in this study. We cannot exclude the possibility that AVE enhances UCP-2 expression through the PPARγ pathway. In addition, we used volume of subarachnoid blood grading system to evaluate the severity of SAH in our model. However, ICP or CPP would also be valuable measurements to assess severity of SAH, especially the EBI. These two parameters are needed to be considered in the future study design. We would like to address these issues in our future study.

In conclusion, we demonstrated that intranasal administration of AVE attenuated oxidative stress and neuronal apoptosis through Mas/PKA/CREB/UCP-2 pathway in EBI after SAH. AVE may be a useful new therapeutic strategy against oxidative stress and neuronal apoptosis in SAH patients.

Declaration of interest

The authors declare that they have no conflict of interest.

Acknowledgments

Appendix A. Supplementary material

Supplementary data associated with this article can be found in the online version at doi:10.1016/j.redox.2018.09.022.

References

[1] H. Suzuki, F. Nakano, To improve translational research in subarachnoid hemorrhage, Transl. Stroke Res. 9 (2018) 1–3.

[2] W.J. Cahill, J.H. Calvert, J.H. Zhang, Mechanisms of early brain injury after subarachnoid hemorrhage, J. Cereb. Blood Flow. Metab. 26 (2006) 1341–1353.

[3] J. Pang, Y. Chen, L. Kuai, et al., Inhibition of blood-brain barrier disruption by an apolipoprotein E-mimetic peptide ameliorates early brain injury in experimental subarachnoid hemorrhage, Transl. Stroke Res. 8 (2017) 257–272.

[4] R.P. Ostrowski, A.R. Colohan, J.H. Zhang, Molecular mechanisms of early brain injury after subarachnoid hemorrhage, Neurol. Res. 28 (2006) 399–414.

[5] R.E. Ayer, J.H. Zhang, Oxidative stress in subarachnoid haemorrhage: significance in acute brain injury and vasospasm, Acta Neurochir. Suppl. 104 (2008) 33–41.

[6] P.G. Matz, J.C. Copin, P.H. Chan, Cell death after exposure to subarachnoid hemolysate correlates inversely with expression of CuZn–superoxide dismutase, Stroke 31 (2000) 2450–2459.

[7] F. Marzatico, P. Gaetani, C. Cafe', et al., Antioxidant enzymatic activities after experimental subarachnoid hemorrhage in rats, Acta Neurol. Scand. 87 (1993) 62–66.

[8] G. Fiskum, R.E. Rosenthal, V. Vereczki, et al., Protection against ischemic brain injury by inhibition of mitochondrial oxidative stress, J. Bioenerg. Biomembr. 36 (2004) 347–352.

[9] R.J. Mailloux, Teaching the fundamentals of electron transfer reactions in mitochondria and the production and detection of reactive oxygen species, Redox Biol. 4 (2015) 381–398.

[10] J.N. Cobley, M.L. Fiorello, D.M. Bailey, 13 reasons why the brain is susceptible to oxidative stress, Redox Biol. 15 (2018) 490–503.

[11] S. Figueroa, M.J. Oset-Gasque, C. Arce, et al., Mitochondrial involvement in nitric oxide-induced cellular death in cortical neurons in culture, J. Neurosci. Res. 83 (2006) 441–449.

[12] G. Mattiasson, P.G. Sullivan, The emerging functions of UCP2 in health, disease, and therapeutics, Antioxid. Redox Signal. 8 (2006) 1–38.

[13] P. Ježek, B. Holendová, K.D. Garlid, et al., Mitochondrial uncoupling proteins: subtle regulators of cellular redox signaling, Antioxid. Redox Signal. 29 (2018) 667–714.

[14] K.P. Normoyle, M. Kim, A. Farahvar, et al., The emerging neuroprotective role of mitochondrial uncoupling protein-2 in traumatic brain injury, Transl. Neurosci. 6 (2015) 179–186.

[15] Z.B. Andrews, S. Diano, T.L. Horvath, Mitochondrial uncoupling proteins in the CNS: in support of function and survival, Nat. Rev. Neurosci. 6 (2005) 829–840.

[16] M. Bader, N. Alenina, M.A. Andrade-Navarro, et al., Mas and its related G protein–coupled receptors, Mrgprs, Pharmacol. Rev. 66 (2014) 1080–1105.

[17] T. Jiang, L. Gao, J. Lu, et al., ACE2-Ang-(1-7)-Mas axis in brain: a potential target for prevention and treatment of ischemic stroke, Curr. Neuropharmacol. 11 (2013) 209–217.

[18] R.W. Regenhardt, F. Desland, A.P. Mecca, et al., Anti-inflammatory effects of angiotensin-(1-7) in ischemic stroke, Neuropharmacology 71 (2013) 154–163.

[19] D.M. Bennion, E. Haltigan, A.J. Irwin, et al., Activation of the neuroprotective angiotensin converting enzyme 2 in rat ischemic stroke, Hypertension 66 (2015) 141–148.

[20] R.A.S. Santos, A.C.S. e. Silva, C. Maric, et al., Angiotensin-(1–7) is an endogenous ligand for the G protein-coupled receptor Mas, Proc. Natl. Acad. Sci. Usa. 100 (2003) 8258–8263.

[21] K. Yamada, S.N. Iyer, M.C. Chappell, et al., Converting enzyme determines plasma clearance of Angiotensin-(1–7), Hypertension 32 (1998) 496–502.

[22] R.A.S. Santos, A.J. Ferreira, Pharmacological effects of AVE 0991, a nonpeptide Angiotensin-(1–7) receptor agonist, Cardiovasc. Drug. Rev. 24 (2006) 239–246.

[23] G. Wiemer, L.W. Dobrucki, F.R. Louka, et al., AVE 0991, a nonpeptide mimic of the effects of Angiotensin-(1–7) on the endothelium, Hypertension 40 (2002) 847–852.

[24] D.S. Skiba, R. Nosalski, T.P. Mikolajczyk, et al., Anti-atherosclerotic effect of the angiotensin 1–7 mimetic AVE0991 is mediated by inhibition of perivascular and plaque inflammation in early atherosclerosis, Br. J. Pharmacol. 174 (2017) 4055–4069.

[25] S. Lee, M.A. Evans, H.X. Chu, et al., Effect of a selective Mas receptor agonist in cerebral ischemia in vitro and in vivo, PLoS One 10 (2015) e0142087.

[26] S.V. Brant Pinheiro, A.C. Simões e Silva, W.O. Sampaio, et al., Nonpeptide AVE 0991 is an angiotensin-(1–7) receptor Mas agonist in the mouse kidney, Hypertension 44 (2004) 490–496.

[27] B. Enkhjargal, D.W. McBride, A. Manaenko, et al., Intranasal administration of vitamin D attenuates blood–brain barrier disruption through endogenous upregulation of osteopontin and activation of CD44/P-gp glycosylation signaling after subarachnoid hemorrhage in rats, J. Cereb. Blood Flow. Metab. 37 (2017) 2555–2566.

[28] T. Sugawara, R. Ayer, V. Jadhav, et al., A new grading system evaluating bleeding scale in filament perforation subarachnoid hemorrhage rat model, J. Neurosci. Methods 167 (2008) 327–334.

[29] J. Yu, X. Li, N. Matei, et al., Ezetimibe, a NPC1L1 inhibitor, attenuates neuronal apoptosis through AMPK dependent autophagy activation after MCAO in rats, Exp. Neurol. 307 (2018) 12–23.

[30] K. Zhou, B. Enkhjargal, Z. Xie, et al., Dihydrolipoic acid inhibits lysosomal rupture and NLRP3 through lysosome-associated membrane protein-1/calcium/calmodulin-dependent protein kinase II/TAK1 pathways after subarachnoid hemorrhage in rat, Stroke 49 (2018) 175–183.

[31] Y. Jiang, J. Wang, D.M. Rozewski, et al., Sensitive liquid chromatography/mass spectrometry methods for quantification of pomalidomide in mouse plasma and brain tissue, J. Pharm. Biomed. Anal. 88 (2014) 262–268.

[32] Z. Xie, B. Enkhjargal, L. Wu, et al., Exendin-4 attenuates neuronal death via GLP-

1R/PI3K/Akt pathway in early brain injury after subarachnoid hemorrhage in rats, Neuropharmacology 128 (2017) 142–151.

[33] K. Bromley-Brits, Y. Deng, W. Song, Morris water maze test for learning and memory deficits in Alzheimer's disease model mice, J. Vis. Exp. (2011) e2920.

[34] N. Xu, Y. Zhang, D.M. Doycheva, et al., Adiponectin attenuates neuronal apoptosis induced by hypoxia-ischemia via the activation of AdipoR1/APPL1/LKB1/AMPK pathway in neonatal rats, Neuropharmacology 133 (2018) 415–428.

[35] R. Wang, W. Ma, G. Gao, et al., Fluoro jade-C staining in the assessment of brain injury after deep hypothermia circulatory arrest, Brain Res. 1372 (2011) 127–132.

[36] B. Lin, Y. Hasegawa, K. Takane, et al., High-Fat-Diet intake enhances cerebral amyloid angiopathy and cognitive impairment in a mouse model of Alzheimer's disease, independently of metabolic disorders, J. Am. Heart Assoc. 5 (2016) e003154.

[37] T. Mahmood, P.C. Yang, Western blot: technique, theory, and trouble shooting, N. Am. J. Med. Sci. 4 (2012) 429–434.

[38] S. Swarnabala, M. Gattu, B. Perry, et al., ROMO1 links oxidative stress to mitochondrial integrity, J. Cell Commun. Signal. 9 (2015) 73–75.

[39] C. Delattre, C. Bournonville, F. Auger, et al., Hippocampal deformations and entorhinal cortex atrophy as an anatomical signature of long-term cognitive impairment: from the MCAO rat model to the stroke patient, Transl. Stroke Res. 9 (2018) 294–305.

[40] R.S. Balaban, S. Nemoto, T. Finkel, Mitochondria, oxidants, and aging, Cell 120 (2005) 483–495.

[41] N. Li, M. Karaca, P. Maechler, Upregulation of UCP2 in beta-cells confers partial protection against both oxidative stress and glucotoxicity, Redox Biol. 13 (2017) 541–549.

[42] B.E. Lonze, D.D. Ginty, Function and regulation of CREB family transcription factors in the nervous system, Neuron 35 (2002) 605–623.

[43] F. Jiang, J. Yang, Y. Zhang, et al., Angiotensin-converting enzyme 2 and angiotensin 1-7: novel therapeutic targets, Nat. Rev. Cardiol. 11 (2014) 413–426.

[44] P. Xu, S. Sriramula, E. Lazartigues, ACE2/ANG-(1–7)/Mas pathway in the brain: the axis of good, Am. J. Physiol. Regul. Integr. Comp. Physiol. 300 (2011) R804–R817.

[45] J. Lu, T. Jiang, L. Wu, et al., The expression of angiotensin-converting enzyme 2–angiotensin-(1–7)–Mas receptor axis are upregulated after acute cerebral ischemic stroke in rats, Neuropeptides 47 (2013) 289–295.

[46] A.Y.W. Chang, F.C.H. Li, C.W. Huang, et al., Interplay between brain stem angiotensins and monocyte chemoattractant protein-1 as a novel mechanism for pressor response after ischemic stroke, Neurobiol. Dis. 71 (2014) 292–304.

[47] K. Duris, A. Manaenko, H. Suzuki, et al., Alpha7 nicotinic acetylcholine receptor agonist PNU-282987 attenuates early brain injury in a perforation model of subarachnoid hemorrhage in rats, Stroke 42 (2011) 3530–3536.

[48] H. Suzuki, Y. Hasegawa, K. Kanamaru, et al., Mechanisms of Osteopontin-induced stabilization of blood-brain barrier disruption after subarachnoid hemorrhage in rats, Stroke 41 (2010) 1783–1790.

[49] Z. Xie, B. Enkhjargal, C. Reis, et al., Netrin-1 preserves blood-brain barrier integrity through deleted in Colorectal Cancer/Focal Adhesion kinase/RhoA signaling pathway following subarachnoid hemorrhage in rats, J. Am. Heart Assoc. 6 (2017) e005198.

[50] A.J. Ferreira, B.A. Jacoby, C.A.A. Araújo, et al., The nonpeptide angiotensin-(1–7) receptor Mas agonist AVE-0991 attenuates heart failure induced by myocardial infarction, Am. J. Physiol. Heart Circ. Physiol. 292 (2007) H1113–H1119.

[51] T. Jiang, L. Gao, J. Shi, et al., Angiotensin-(1-7) modulates renin–angiotensin system associated with reducing oxidative stress and attenuating neuronal apoptosis in the brain of hypertensive rats, Pharmacol. Rev. 67 (2013) 84–93.

[52] Y. Zhang, J. Liu, J.Y. Luo, et al., Upregulation of angiotensin (1-7)-mediated signaling preserves endothelial function through reducing oxidative stress in diabetes, Antioxid. Redox Signal. 23 (2015) 880–892.

[53] L.A. Rabelo, N. Alenina, M. Bader, ACE2–angiotensin-(1–7)–Mas axis and oxidative stress in cardiovascular disease, Hypertens. Res. 34 (2011) 154–160.

[54] O. Bendel, T. Bueters, M. von Euler, et al., Reappearance of hippocampal CA1 neurons after ischemia is associated with recovery of learning and memory, J. Cereb. Blood Flow. Metab. 25 (2005) 1586–1595.

[55] K. Hellner, T. Walther, M. Schubert, et al., Angiotensin-(1–7) enhances LTP in the hippocampus through the G-protein-coupled receptor Mas, Mol. Cell. Neurosci. 29 (2005) 427–435.

[56] L.S. Lara, D. Vives, J.S. Correa, et al., PKA-mediated effect of MAS receptor in counteracting angiotensin II-stimulated renal Na + -ATPase, Arch. Biochem. Biophys. 496 (2010) 117–122.

[57] K. Søberg, L.V. Moen, B.S. Skålhegg, et al., Evolution of the cAMP-dependent protein kinase (PKA) catalytic subunit isoforms, PLoS One 12 (2017) e0181091.

[58] R.E. Turnham, J.D. Scott, Protein kinase A catalytic subunit isoform PRKACA; History, function and physiology, Gene 577 (2016) 101–108.

[59] R. Tanaka, Alteration of second messengers during acute cerebral ischemia–adenylate cyclase, cyclic AMP-dependent protein kinase, and cyclic AMP response element binding protein, Prog. Neurobiol. 65 (2001) 173–207.

[60] G. Mattiasson, M. Shamloo, G. Gido, et al., Uncoupling protein-2 prevents neuronal death and diminishes brain dysfunction after stroke and brain trauma, Nat. Med. 9 (2003) 1062–1068.

[61] S.L. Mehta, P.A. Li, Neuroprotective role of mitochondrial uncoupling protein 2 in cerebral stroke, J. Cereb. Blood Flow. Metab. 29 (2009) 1069–1078.

[62] Z.B. Andrews, Z.W. Liu, N. Walllingford, et al., UCP2 mediates ghrelin's action on NPY/AgRP neurons by lowering free radicals, Nature 454 (2008) 846–851.

[63] I. Bechmann, S. Diano, C.H. Warden, et al., Brain mitochondrial uncoupling protein 2 (UCP2): a protective stress signal in neuronal injury, Biochem. Pharmacol. 64 (2002) 363–367.

[64] K. Yamamizu, T. Matsunaga, S. Katayama, et al., PKA/CREB signaling triggers initiation of endothelial and hematopoietic cell differentiation via Etv2 induction, Stem Cells 30 (2012) 687–696.